

2D vs. 3D BAO: quantification of their tension and test of the Etherington relation

Arianna Favale^{a,b}, Adrià Gómez-Valent^b, Marina Migliaccio^a

^a*Dipartimento di Fisica and INFN Sezione di Roma 2, Università di Roma Tor Vergata, via della Ricerca Scientifica 1, Roma, 00133, Italy*

^b*Departament de Física Quàntica i Astrofísica and Institut de Ciències del Cosmos, Universitat de Barcelona, Av. Diagonal 647, Barcelona, 08028, Spain*

Abstract

Several studies in the literature have found a disagreement between compressed data on Baryon Acoustic Oscillations (BAO) derived using two distinct methodologies: the two-dimensional (2D, transverse or angular) BAO, which extracts the BAO signal from the analysis of the angular two-point correlation function; and the three-dimensional (3D or anisotropic) BAO, which also exploits the radial clustering signal imprinted on the large-scale structure of the universe. This discrepancy is worrisome, since many of the points contained in these data sets are obtained from the same parent catalogs of tracers and, therefore, we would expect them to be consistent. Since BAO measurements play a pivotal role in the building of the inverse distance ladder, this mismatch impacts the discourse on the Hubble tension and the study of theoretical solutions to the latter. So far, the discrepancy between 2D and 3D BAO has been only pointed out in the context of fitting analyses of cosmological models or parametrizations that, in practice, involve the choice of a concrete calibration of the comoving sound horizon at the baryon-drag epoch. In this Letter, for the first time, we quantify the tension in a much cleaner way, with the aid of apparent magnitudes of supernovae of Type Ia and excluding the radial component of the 3D BAO. We avoid the use of any calibration and cosmological model in the process. At this point we assume that the Etherington (a.k.a distance duality) relation holds. We use state-of-the-art measurements in our analysis, and study how the results change when the angular components of the 3D BAO data from BOSS/eBOSS are substituted by the recent data from DESI Y1. We find the tension to exist at the level of $\sim 2\sigma$ and $\sim 2.5\sigma$, respectively. In view of this result, we then apply a calibrator-independent method to investigate the robustness of the distance duality relation when analyzed not only with 3D BAO measurements, but also with 2D BAO. This is a test of fundamental physics, which covers, among other aspects, variations of the speed of light with the cosmic expansion or possible interactions between the dark and electromagnetic sectors. We do not find any hint for a violation of the cosmic distance duality relation in any of the considered data sets, although they leave still room for departures from it.

Keywords: distance ladder, baryon acoustic oscillations, cosmological tensions, tests of Λ CDM

1. Introduction

Baryon Acoustic Oscillations (BAO), as standardizable rulers, and Supernovae of Type Ia (SNIa), as standardizable candles, stand out as two pivotal observational tools in cosmology. They were crucial for the discovery (Riess et al., 1998; Perlmutter et al., 1999) and subsequent characterization of the late-time acceleration of the universe (Cole et al., 2005; Eisenstein et al., 2005) and, hence, for the consolidation of Λ CDM as the current standard cosmological model (Peebles and Ratra, 2003; Padmanabhan, 2003; Turner, 2022). BAO and SNIa are a source of precious background information (Alam et al., 2021; Brout et al., 2022; Rubin et al., 2023; Vincenzi et al., 2024; Adame et al., 2024c). They are excellent independent probes of the geometry and energy content of the universe, complementary to Cosmic Microwave Background (CMB) experiments (Aghanim et al., 2020; Aiola et al., 2020), weak gravitational lensing measurements (Abbott et al., 2023) and a plethora of emerging cosmological probes like cosmic chronometers,

gamma-ray bursts or quasars, among others (Moresco et al., 2022).

Importantly, SNIa and BAO are also instrumental in the discussion of the Hubble tension. The mismatch between the direct cosmic distance ladder measurement of H_0 by the SH0ES Team (Riess et al., 2022), which is model-independent, and the value inferred by the *Planck* Collaboration from the analysis of the CMB temperature, polarization and lensing spectra assuming Λ CDM (Aghanim et al., 2020) is already reaching the 5σ level. When combined with SNIa, anisotropic (or 3D) BAO, calibrated with the value of the comoving sound horizon at the baryon-drag epoch measured by *Planck* considering standard physics before the decoupling time ($r_d \sim 147$ Mpc), lead to values of H_0 fully in accordance with the Planck/ Λ CDM estimate, rendering the tension with the local measurement high, see e.g. (Bernal et al., 2016; Feeney et al., 2019; Lemos et al., 2019). This method for estimating H_0 using r_d as an anchor is known as the inverse distance ladder (IDL). The only way to reconcile the IDL result obtained with 3D BAO with the SH0ES measurement keeping standard pre-recombination physics is by a sudden growth of the SNIa absolute magnitude accompanied by a fast phantom-like increase of $H(z)$ at $z \lesssim 0.1$ (Alesta

Email addresses: afavale@roma2.infn.it (Arianna Favale), agomezvalent@icc.ub.edu (Adrià Gómez-Valent), migliaccio@roma2.infn.it (Marina Migliaccio)

et al., 2021, 2022; Gómez-Valent et al., 2024; Tutusaus et al., 2023; Bousis and Perivolaropoulos, 2024), while sticking to the Planck/ Λ CDM behavior at higher redshifts. It is well-known that a phantom transition alone cannot solve this problem (Benevento et al., 2020; Camarena and Marra, 2021; Efsthathiou, 2021; Heisenberg et al., 2022). Alternatively, a very local transition in the SNIa absolute magnitude at $z \lesssim 0.01$ (Marra and Perivolaropoulos, 2021; Perivolaropoulos, 2022; Perivolaropoulos and Skara, 2022; Ruchika et al., 2023) or the existence of unaccounted for systematic effects in the second rung of the direct distance ladder could also do the job (Wojtak et al., 2023; Wojtak and Hjorth, 2024).

Paradoxically, when the IDL is built using angular (transversal or 2D) BAO data one gets a very different answer (Camarena and Marra, 2020). In this case, one can explain with late-time new physics the large values of the Hubble constant and absolute magnitude of SNIa measured by SH0ES respecting the constancy of the latter (Gómez-Valent et al., 2024). The effective dark energy density must become, though, negative at $z \gtrsim 2$ and, hence, transversal BAO require new physics at much higher redshifts (Gómez-Valent et al., 2024)¹. Akarsu et al. (2023) have found that, in the context of a model with a sign-switching cosmological constant, it is possible to get rid of the H_0 and growth tensions when angular BAO is employed in the fitting analysis, instead of 3D BAO (see also Anchordoqui et al. 2024). Fitting results improve even more if dark energy is of quintessence type at late times, after the transition, something that can be realized in the model with phantom matter proposed by Gómez-Valent and Solà Peracaula (2024). Interestingly, a negative cosmological constant could also induce a larger abundance of extremely massive galaxies at $z \gtrsim 5$ and, therefore, have a positive bearing on the tension with the data from the *James Webb Space Telescope* (Adil et al., 2023; Menci et al., 2024). Analyses of interacting dark energy carried out with 2D and 3D BAO data lead to completely inconsistent results too (Bernui et al., 2023).

The aforementioned conflict between anisotropic and angular BAO data is evident from Fig. 1. It clearly points to the existence of unknown systematic errors affecting one or both BAO data sets, or to an underestimation of their uncertainties. 2D BAO analyses make use of the angular two-point correlation function or the angular power spectrum, and measure the angular position of the BAO peak. They do not require the use of a fiducial model to convert redshifts and angles into positions in a 3D tracer map (Sánchez et al., 2011). This is why it is usually claimed to be only weakly dependent on a cosmological model (see e.g. de Carvalho et al. 2021).

Anisotropic BAO, instead, employ a fiducial cosmological model to build the 3D maps of tracers in redshift space. The impact of the fiducial cosmology has been demonstrated to induce only small shifts in the inferred cosmological distances

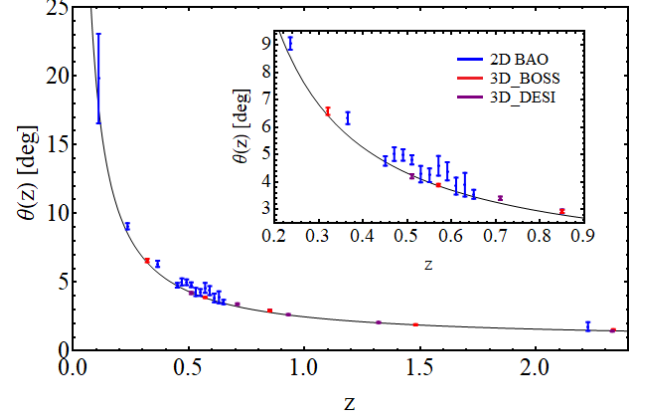


Figure 1: 2D and 3D BAO measurements of $\theta(z) = r_d/D_M(z)$, see Tables 1 and 2, and Sec. 2. In black, we show the theoretical curve obtained with the best-fit Planck/ Λ CDM model (TT,TE,EE+lowE+lensing analysis, Aghanim et al. 2020). The inner plot shows a zoom in the redshift range $z \in [0.2, 0.9]$.

when it does not differ significantly from the true model (Carter et al., 2020; Heinesen et al., 2020; Bernal et al., 2020; Pan et al., 2023; Sanz-Wuhl et al., 2024). However, Anselmi et al. (2019) showed that fitting the two-point function while fixing the cosmological and the non-linear-damping parameters at fiducial values leads to an underestimation of the errors by a factor of two, which could certainly mitigate the tension between the 3D and 2D BAO measurements.

While this discrepancy as well as its impact on the Hubble tension has been pointed out previously in the literature (Camarena and Marra, 2020; Gómez-Valent et al., 2024), so far there has been no accurate quantification of the statistical tension between these two BAO data sets. In this work, we provide a method to perform this quantification in a quite model-independent way. We apply it to state-of-the-art BAO data, including the anisotropic measurements reported by DESI in their first year release, and compare these results with those obtained using the 3D BAO data from BOSS/eBOSS. Moreover, we also study the effect of a possible underestimation of the 3D BAO uncertainties on our results. This is motivated by the work by Anselmi et al. (2019).

In the first part of the Letter we take the fulfillment of the Etherington relation (Etherington, 1933), a.k.a distance duality relation (DDR), for granted. In terms of the redshift z , the latter reads,

$$D_L(z) = (1+z)^2 D_A(z), \quad (1)$$

with $D_L(z)$ and $D_A(z)$ the luminosity and angular diameter distances, respectively. The Etherington relation holds in metric theories of gravity with photons conserved and propagating in null geodesics. Thus, any deviation from this relation, which would imply that

$$\eta(z) \equiv \frac{D_L(z)}{(1+z)^2 D_A(z)} \neq 1 \quad (2)$$

in some redshift range(s), would hint at new physics either in the gravity sector or beyond the standard model of particle

¹Huang et al. (2024) reach a different conclusion. This is due to the fact that they do not use the constraint on the angular diameter distance to the last scattering surface $D_A(z_*)$, which is crucial to build the IDL consistently with the assumption of standard pre-recombination physics and the precise measurement of θ_* by the *Planck* mission.

Survey	z	D_A/r_d	References
DES Y6	0.85	10.58 ± 0.21	Abbott et al. (2024)
BOSS DR12	0.32	6.5986 ± 0.1337	Gil-Marín et al. (2017)
	0.57	9.389 ± 0.103	
eBOSS DR16Q	1.48	12.18 ± 0.32	Hou et al. (2020)
Ly α -F eBOSS DR16	2.334	$11.25^{+0.36}_{-0.33}$	du Mas des Bourboux et al. (2020)
LRG1 DESI Y1	0.51	9.02 ± 0.17	Adame et al. (2024a)
LRG2 DESI Y1	0.71	9.85 ± 0.19	Adame et al. (2024a)
LRG3+ELG1 DESI Y1	0.93	11.25 ± 0.16	Adame et al. (2024a)
ELG2 DESI Y1	1.32	11.98 ± 0.30	Adame et al. (2024a)
Ly α -F DESI Y1	2.33	11.92 ± 0.29	Adame et al. (2024b)

Table 1: List with the anisotropic BAO data points used in this work. See the quoted references for details. As explained in Sec. 2, we use two alternative anisotropic BAO data sets, one containing the DES Y6 and BOSS/eBOSS data points, and another one that combines the DES Y6 and DESI Y1 data.

physics. Among other possibilities, this could be the case of models with a time-varying speed of light (see e.g. Lee 2021; Gupta 2023) or theories with a coupling between photons and fields in the dark sector, e.g. with axions or axion-like particles (see e.g. Jaeckel and Ringwald (2010); Carosi et al. (2013)). Of course, these deviations could also hint at the existence of unknown systematic errors in the data.

Tests of the Etherington relation have been carried out using SNIa in combination with 3D BAO (More et al., 2009; Nair et al., 2012; Ma and Corasaniti, 2018; Martinelli et al., 2020; Renzi et al., 2022), cosmic chronometers (Avgoustidis et al., 2010) or data on compact radio quasars (Tonghua et al., 2023), and even with luminosity distances from high-redshift quasars and data from strong gravitational lenses (Qin et al., 2021). See also (Qi et al., 2019). No significant deviation from the DDR has been found so far. In view of the tension between the 2D and 3D BAO data sets, we deem interesting and very timely to also study what happens if we employ angular BAO, instead of 3D BAO, to test the Etherington relation and see whether the tension between these two data sets reflects also into differences at the level of the DDR. Moreover, we will compare the results obtained with anisotropic BAO from BOSS/eBOSS and DESI Y1 to determine if conclusions on the validity of the Etherington relation have changed with the new data.

This Letter is structured as follows. In Sec. 2 we explain the methodology and the data sets employed in our analyses. We describe the method used to quantify the tension between the angular and anisotropic BAO measurements and also the calibrator-independent test of the Etherington relation. In Sec. 3 we present our results and discuss how they change when we substitute the BOSS/eBOSS data by the recent DESI data. Finally, in Sec. 4 we present our conclusions and outlook.

2. Methodology and data

The relation between the luminosity distance and the apparent magnitude m of a standard candle is given by

$$m(z) = M + 25 + 5 \log_{10} \left(\frac{D_L(z)}{1 \text{ Mpc}} \right), \quad (3)$$

where M is its absolute magnitude. Along this paper, we employ SNIa as standard candles. We make use of the Pantheon+ compilation (Scolnic et al., 2022), which is a collection of 1701 lightcurves of 1550 distinct SNIa. In particular, we consider a subsample of 1624 data points, since we do not include those SNIa lying in Cepheid host galaxies, although we have explicitly checked that the impact of these objects on our results is completely negligible.

On the other hand, we use the comoving sound horizon r_d as a cosmic standard ruler. Galaxy surveys have been able to measure the angle

$$\theta(z) = \frac{r_d}{D_M(z)} \quad (4)$$

at various redshifts, with $D_M(z) = (1+z)D_A(z)$ the comoving angular diameter distance. We employ the angular and anisotropic BAO data listed in Tables 1 and 2, respectively. In the case of the 3D BAO, we use two alternative data sets: one combines the DES Y6 and BOSS/eBOSS data sets, whereas the other substitutes the latter by the DESI Y1 data. We refer to these two data sets as 3D_BOSS and 3D_DESI, respectively. The BOSS/eBOSS and DESI compressed data points have been obtained from catalogs with partially overlapping population and non-disjoint patches in the sky, so we opt not to combine them and proceed as explained above in order to avoid double counting issues, since the correlations between these two sets of data are not known.

From Eqs. (3) and (4) it is straightforward to write the luminosity and angular diameter distances in terms of the calibrators (M and r_d) and the measured quantities ($m(z)$ and $\theta(z)$). Plugging these expressions into Eq. (2) we obtain,

$$\eta(z) = \frac{10^{m(z)/5} \theta(z)}{(1+z)} \frac{10^{-5-M/5} \text{ Mpc}}{r_d}. \quad (5)$$

If the Etherington relation is fulfilled (i.e., if $\eta(z) = 1$) and if we have measurements of $\theta(z)$ and $m(z)$ at the same redshift, we can compute the degeneracy direction in the calibrators' plane,

$$\bar{r}_d 10^{M/5} = \frac{10^{m(z)/5} \theta(z)}{10^5 (1+z)}, \quad (6)$$

Survey	z	θ_{BAO} [deg]	References
SSDS DR12	0.11	19.8 ± 3.26	de Carvalho et al. (2021)
SDSS DR7	0.235	9.06 ± 0.23	Alcaniz et al. (2017)
	0.365	6.33 ± 0.22	
SDSS DR10	0.45	4.77 ± 0.17	Carvalho et al. (2016)
	0.47	5.02 ± 0.25	
	0.49	4.99 ± 0.21	
	0.51	4.81 ± 0.17	
	0.53	4.29 ± 0.30	
	0.55	4.25 ± 0.25	
SDSS DR11	0.57	4.59 ± 0.36	Carvalho et al. (2020)
	0.59	4.39 ± 0.33	
	0.61	3.85 ± 0.31	
	0.63	3.90 ± 0.43	
	0.65	3.55 ± 0.16	
DES Y6	0.85	2.932 ± 0.068	Abbott et al. (2024)
BOSS DR12Q	2.225	1.77 ± 0.31	de Carvalho et al. (2018)

Table 2: List with the 16 2D BAO data points used in this work, with $\theta_{\text{BAO}}(z)$ [rad] = $r_d/[(1+z)D_A(z)]$. The 2D BAO data point of DES Y6 can be also written as $D_A/r_d = 10.57 \pm 0.24$, which is correlated with the 3D BAO DES Y6 data point of Table 1 with a Pearson correlation coefficient $\rho = 0.896$. See the quoted references for further details.

with $\bar{r}_d \equiv r_d/(1 \text{ Mpc})$ the dimensionless sound horizon. This calculation is independent of the curvature of the universe, which we do not need to specify. We do not have SNIa and BAO data at the very same redshifts, of course, but this is not a major complication, since we can employ some interpolation method to obtain the constrained values of $m(z)$ at the BAO redshifts².

One of these methods is the Gaussian Processes (GP) regression technique (Rasmussen and Williams, 2006), which can be used to reconstruct functions from Gaussian distributed data under very minimal assumptions. Thanks to the definition of a kernel function, which in most cases depends only on two hyperparameters, one can track the correlations between points where data are absent. In principle, one should marginalize over these hyperparameters to account for the propagation of their uncertainties to the reconstructed function. However, due to the large covariance matrix of the SNIa of the Pantheon+ sample, this process is very expensive from a computational point of view. In this work, we opt to follow the same approach already tested in (Favale et al., 2023), where it is shown that differences in the reconstructed shapes obtained with the marginalization and optimization procedures are smaller than 0.1σ in the case under study, thus not impacting significantly the final results. We make use of the publicly available GaPP code developed by Seikel et al. (2012). Using GP we generate $N = 10^4$ samples of SNIa apparent magnitudes at the BAO redshifts z_i . For each redshift z_i , we also draw N realizations of $\theta(z_i)$ from a Gaussian distribution that has as mean the measured value and as standard deviation the associated uncertainty. With this information we can obtain a distribution of N samples of the product $\bar{r}_d 10^{M/5}$ (Eq. 6) at the BAO redshifts. There exist non-null correlations,

since we employ correlated SNIa data and take also into account the correlation between the angular and anisotropic DES Y6 data points (Abbott et al., 2024), see the caption of Table 2. On the other hand, we expect non-zero positive correlations between several data points in the 2D and 3D data samples, simply because they have been obtained from the same parent catalogs of tracers (cf. Tables 1 and 2). However, these correlation coefficients have not been quantified, except in the case of DES, so we cannot use them in our analysis. This fact will lead us to estimate, in practice, a conservative lower bound of the tension between the angular and anisotropic BAO data sets.

The next step is to estimate representative values of $\bar{r}_d 10^{M/5}$ for the 2D and 3D BAO data sets. To do so we need to obtain first their distribution out of the Markov chain. This will allow us to quantify the tension between the two data sets, by means of the tension between the corresponding values of $\bar{r}_d 10^{M/5}$. As a starting point, we employ the so-called Edgeworth expansion (see Amendola (1996) and references therein) to compute an analytical approximation of the underlying (exact) distribution,

$$f(\vec{x}) = G(\vec{x}, \lambda) \left[1 + \frac{1}{6} k^{ijk} h_{ijk}(\vec{x}, \lambda) + \dots \right], \quad (7)$$

which is a multivariate function with the same dimensionality as the total number of BAO data points contained in the 3D and 2D data sets. This expression is valid when the departures from Gaussianity are sufficiently small. The second term inside the brackets and the dots account for non-Gaussian corrections. We have explicitly checked that in the case under study it is more than sufficient to keep only the first correction. In Eq. (7), $x^i = d^i - \mu^i$, with $d^i = \bar{r}_d 10^{M/5}|_i$ and $\vec{\mu}$ the mean vector, i.e. $\mu^i = \langle \bar{r}_d 10^{M/5}|_i \rangle$. The subscript i labels the BAO data point, which can belong to the 2D or 3D BAO data sets. $\lambda = C^{-1}$ is the inverse of the covariance matrix, with elements $C^{ij} = \langle x^i x^j \rangle$. $G(\vec{x}, \lambda)$ is the multivariate Gaussian distribution built

²Interpolating the BAO data to obtain the BAO constraints at the SNIa redshifts is also possible, but introduces a much larger uncertainty, since BAO are much more sparse. Thus, this is not the most optimal way to proceed.

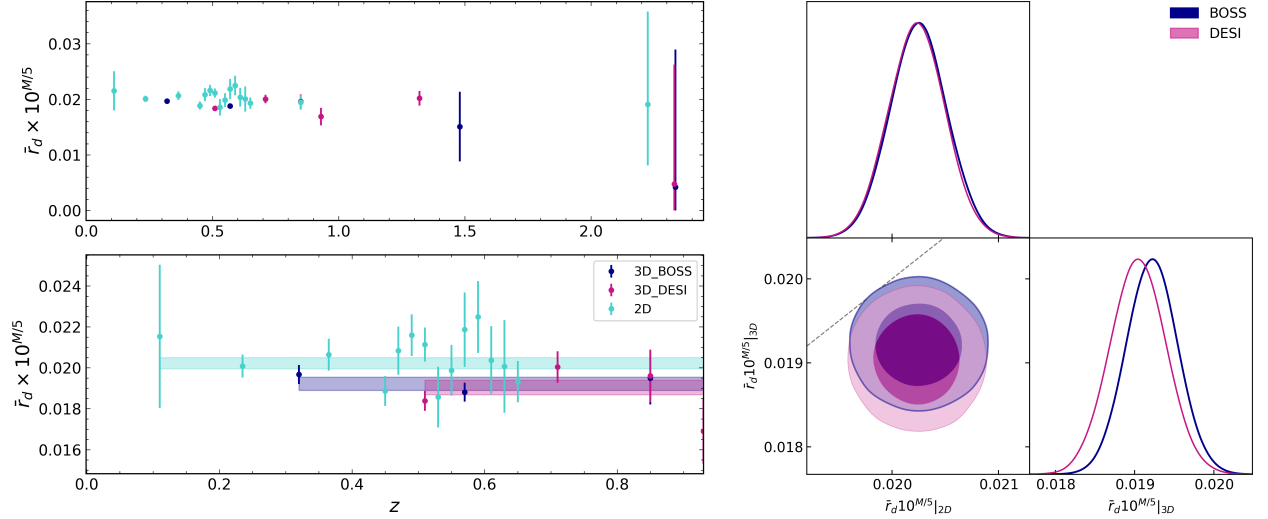


Figure 2: *Left upper plot:* Constraints at 68% C.L. on the product $\bar{r}_d \times 10^{M/5}$ obtained making use of the SNIa contained in the Pantheon+ compilation and the individual 3D and 2D BAO data points, assuming the validity of the Etherington relation. We follow the method explained in Sec. 2. *Lower left plot:* Same as the left upper plot, but with a zoom in the range $z \in [0, 0.95]$. The horizontal bands represent the 2D, 3D_BOSS and 3D_DESI BAO constraints at 68% C.L. *Right plot:* The corresponding triangle plot, with the contours at 68% and 95% C.L. The dashed straight line in grey $\bar{r}_d \cdot 10^{M/5}|_{3D} = \bar{r}_d \cdot 10^{M/5}|_{2D}$ represents the null hypothesis of consistency between the 3D and 2D BAO data sets.

from that mean and covariance matrix, and $k^{ijk} = \langle x^i x^j x^k \rangle$ are the elements of the so-called skewness matrix. Finally,

$$h_{ijk}(\vec{x}) = \lambda_{in}\lambda_{jt}\lambda_{kl}x^n x^t x^l - (\lambda_{ij}\lambda_{kt} + \lambda_{ik}\lambda_{jt} + \lambda_{jk}\lambda_{it})x^t \quad (8)$$

is the Hermite tensor of order 3. In Eqs. (7) and (8) we have employed Einstein's summation convention. All these objects can be directly computed from the chain. Once we build the distribution of Eq. (7), we can sample it treating it as a two-dimensional distribution for $\bar{r}_d 10^{M/5}$, with one dimension for the 2D BAO data set, and the other for the 3D BAO data set, i.e. $f(x_{2D}, x_{3D})$. When the non-Gaussian features are negligible, the resulting distribution reduces of course to a Gaussian with the following weighted mean vector $\tilde{\mu}$ and inverse covariance matrix $\tilde{\lambda}$,

$$\tilde{\mu}_I = \tilde{\lambda}_{IJ}^{-1} v_J \quad ; \quad \tilde{\lambda}_{IJ} = \sum_{i \in I} \sum_{j \in J} \lambda_{ij}, \quad (9)$$

with

$$v_I = \sum_{i \in I} \sum_{j=1}^N \lambda_{ij} \mu_j \quad (10)$$

and N the total number of BAO data points contained in the 2D and 3D data sets. If we perform the analysis with 3D_BOSS, $N = 21$; if, instead, we use 3D_DESI, $N = 22$. Here we have indicated sums over all the elements contained in the data set I as $\sum_{i \in I}$, with I referring to the 2D or 3D BAO data sets.

To quantify the tension between the anisotropic and angular BAO data we can just build the histogram of $\chi^2 = -2 \ln f(x_{2D}, x_{3D})$ resulting from the sampling of the two-dimensional distribution obtained with the procedure described

BAO data set	$\bar{r}_d 10^{M/5}$	p -value
2D	$(20.25 \pm 0.27) \cdot 10^{-3}$	–
3D_BOSS	$(19.22 \pm 0.32) \cdot 10^{-3}$	0.052 ± 0.007
	$(19.12 \pm 0.46) \cdot 10^{-3}$	$0.098^{+0.019}_{-0.007}$
3D_DESI	$(19.04 \pm 0.35) \cdot 10^{-3}$	0.029 ± 0.006
	$(19.08 \pm 0.49) \cdot 10^{-3}$	$0.114^{+0.021}_{-0.005}$

Table 3: Constraints at 68% C.L. on the product $\bar{r}_d 10^{M/5}$ for the 2D and 3D BAO data sets, following the procedure explained in Sec. 2. They incorporate possible deviations from Gaussianity, encapsulated in Eq. (7), which are, in any case, derisory, as we have explicitly checked by comparing these results with those obtained with Eqs. (9)-(10). The level of tension between the 2D and 3D BAO data sets is quantified by the p -value, reported in the last column of the table. In the second rows of 3D_BOSS and 3D_DESI, we present the results obtained by doubling the uncertainties associated with the 3D BAO measurements.

above, and then compute the p -value associated to the hypothesis of having only one single BAO data set (built out from the joint 2D and 3D BAO data sets). In point of fact, we can obtain the full distribution of p -values, which allows us to compute also the associated uncertainty. The smaller the p -value, the more the hypothesis is excluded, of course, indicating greater inconsistency between the two data sets. We repeat this exercise with both 3D_BOSS and 3D_DESI (one at a time) in combination with 2D BAO to determine if the level of tension between the angular and the anisotropic BAO data sets changes. We present the results of this analysis in Sec. 3.1.

In the second part of the analysis, we test the Etherington relation following the calibrator-independent method employed by Tonghua et al. (2023). It is based on the quantity

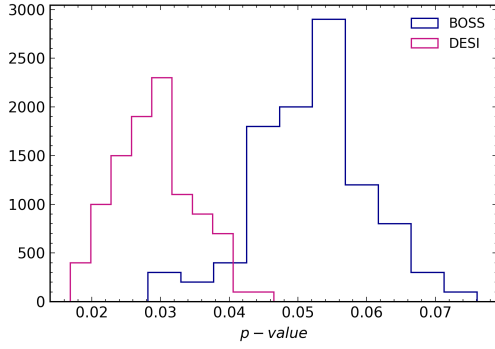


Figure 3: Distribution of p -values from the analyses with 2D BAO+3D_BOSS and 2D BAO+3D_DESI. See Sec. 3.1 for details.

$$\eta_{i,j} \equiv \frac{\eta(z_i)}{\eta(z_j)} = \frac{10^{m(z_i)/5} \theta(z_i)}{10^{m(z_j)/5} \theta(z_j)} \left(\frac{1+z_j}{1+z_i} \right), \quad (11)$$

which is built from the ratio of Eq. (5) at two different redshifts. Avoiding the use of the calibrators of the distance ladders in this test is important not to propagate possible biases that might have been introduced in their measurement. This is relevant on account of the Hubble tension. Departures of $\eta_{i,j}$ from unity could hint at a violation of the DDR, if the deviation from DDR is not constant in redshift. In Sec. 3.2 we show our results obtained with 2D, 3D_BOSS and 3D_DESI BAO, in combination with the SNIa of the Pantheon+ compilation.

3. Results

3.1. Tension between angular and anisotropic BAO

In the left plots of Fig. 2 we show the constraints on the product $\bar{r}_d \times 10^{M/5}$ defined in Eq. (6), obtained by making use of the individual BAO angles in combination with the SNIa apparent magnitudes of Pantheon+. In the lower plot we also present the overall constraints obtained from each BAO data set, see the horizontal bands at 68% C.L. and the results reported in Table 3. The contour plot on the right complements the preceding information and helps to better assess visually the tension between the 2D and 3D BAO data sets. The latter points to a $\sim 2\sigma$ C.L. tension when the anisotropic BOSS data are used, and grows up to the $\sim 2.5\sigma$ C.L. with DESI. The roughly circular shape of the 2D contours responds to the fact that the correlations introduced by SNIa turn out to be very small and we have not considered correlations between the 2D and 3D BAO data sets, apart from those of DES (see Sec. 2).

Following the methodology explained in Sec. 2, we also compute the distribution of p -values associated with the hypothesis of having only one single BAO data set (see Fig. 3). We obtain a p -value of 0.052 ± 0.007 and 0.029 ± 0.006 when employing 3D_BOSS and 3D_DESI, respectively (Table 3). These more quantitative results are fully aligned with those of Fig. 2, of course.

It is of utmost importance to note that this tension, despite not being very high, is still substantial and obtained in a largely

model-independent manner, assuming only the validity of the Etherington relation. The addition of the radial component of the 3D BAO data, which has not been considered in our analysis because it is not feasible to incorporate it following a model- and calibrator-independent approach, increases the tension even more. This explains why fitting analyses with angular and anisotropic BAO data lead to completely different results, as shown in, for example, Bernui et al. (2023). In particular, they require different solutions to the Hubble tension (Gómez-Valent et al., 2024).

Several recent works have pointed out that the DESI BAO data obtained from luminous red galaxies at $z = 0.51$ are possibly driving the signs of dynamical dark energy found by combining DESI with CMB, observational Hubble data and SNIa (Adame et al., 2024c; Colgáin et al., 2024; Carloni et al., 2024; Wang, 2024). It is therefore worthwhile to closely examine these data and their impact on our results. However, the $\sim 2\sigma$ offset of the DESI data at $z = 0.51$ from the Planck/ Λ CDM model reported by Adame et al. (2024a) is only found in the radial measurement, $D_H(z)/r_d = c/H(z)r_d$, i.e. it is not present in the transversal BAO component (see their Figure 15 and also our Fig. 1). The latter is fully consistent with Planck/ Λ CDM, as are the other 3D BAO data. Thus, we can conclude that this data point is not playing a major role in our analysis, apart from tightening the constraint on the product $\bar{r}_d \times 10^{M/5}$ extracted with 3D_DESI.

Finally, motivated by the work by Anselmi et al. (2019), we have also studied to what extent the tension loosens if we increase the uncertainties of the 3D BAO measurements by a factor of two. The results are displayed in Table 3. The p -values are approximately 0.1 in this case when the 2D BAO is combined with both 3D BAO data sets, resulting in a discrepancy of less than 2σ and, hence, in no significant statistical tension. This means that an underestimation of the 3D BAO uncertainties as the one estimated by Anselmi et al. (2019) could mitigate the tension between angular and anisotropic measurements, improving in this way their concordance.

3.2. Test of the Etherington relation

We follow the procedure described in the last part of Sec. 2 to obtain the values of $\eta_{i,i+1}$ (Eq. 11) using the various BAO data sets. For each of them, we compute the following function

$$\tilde{\eta}_I(z) = \sum_{i=1}^{N_I-1} \eta_{i,i+1} \Theta(z - z_i) \Theta(z_{i+1} - z), \quad (12)$$

where $\Theta(\cdot)$ is the Heaviside step function, and we show the resulting 68% C.L. constraints on it in Fig. 4. Eq. (12) accounts for all the independent couples of z . The subscript I labels the BAO data set employed in the calculation and N_I is the number of BAO data points contained in it.

We do not find any significant hint of a violation of the DDR. Regardless of the BAO data set employed in the analysis, the quantity $\tilde{\eta}(z)$ is compatible with 1 at approximately $1 - 2\sigma$ C.L. While this result is consistent with previous analyses using the anisotropic 3D_BOSS data set (see e.g., Renzi et al. 2022), our study represents the first investigation in the literature to test the

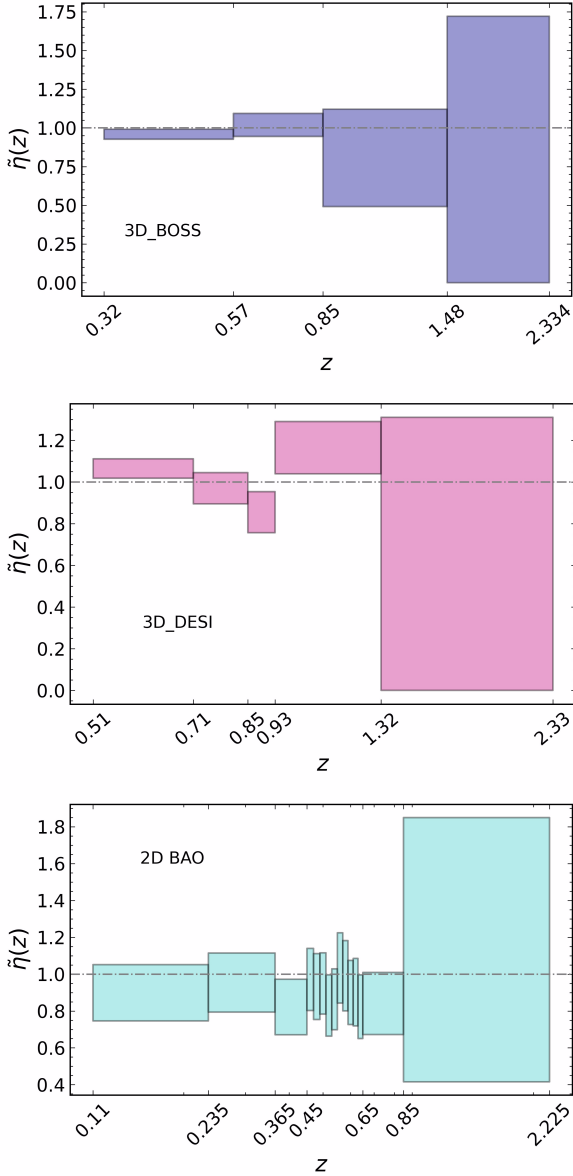


Figure 4: Constraints at 68% C.L. on $\tilde{\eta}(z)$, as defined in Eq. (12), obtained making use of the 3D and 2D BAO data sets in combination with the SNIa of the Pantheon+ compilation. The x-axes are in logarithmic scale for the sake of a better visualization. We write the z values of the various BAO data points employed in the construction of $\tilde{\eta}(z)$, except in the region of redshifts in the 2D BAO plot where the density of points is too high, see Table 2.

DDR using both the 3D DESI Y1 and the 2D BAO data sets. The tension between the anisotropic and angular BAO data sets discussed in Section 3.1 does not manifest as a deviation from the DDR when considering the angular BAO data. To date, uncertainties on $\tilde{\eta}_I(z)$ are still large, especially at high redshift, where they can reach 100% due to large errors in SNIa data.

4. Conclusions and outlook

We have devoted this Letter to the quantification of the existing tension between the angular and anisotropic data on baryon

acoustic oscillations, employing a novel and quite model-independent approach which only relies on the fulfillment of the Etherington relation and is also independent of the calibrators of the direct and inverse distance ladders. The method excludes the radial 3D BAO data, but nevertheless we find a tension at $\sim 2\sigma$ C.L. between the 2D BAO and the anisotropic data set built with DES Y6 and BOSS/eBOSS, which gets enhanced up to $\sim 2.5\sigma$ C.L. when the BOSS/eBOSS data set is substituted by the first data release of DESI. This can be considered a lower bound of the actual tension, also because we cannot account for most of the existing correlations between the 2D and 3D BAO data sets, since they have not been reported in the literature.

The statistical significance of the aforesaid discrepancy would be softened if, for some reason, the BAO uncertainties had been underestimated. This is a plausible possibility according to Anselmi et al. (2019), who found that the errors in standard anisotropic BAO analyses might be underestimated by a factor of two. In order to assess the impact of this underestimation on our results we have repeated the analysis doubling the uncertainties of 3D_BOSS and 3D_DESI and find that the tension decreases below the 2σ C.L., which tells us that the tension between angular and anisotropic BAO is not very relevant if the error bars in the compressed BAO data are not being properly estimated in current analyses. At least, when the radial information is not accounted for.

In view of the existing tension between 2D and 3D BAO, which grows even more in the context of model-dependent analyses thanks to the inclusion of the radial 3D component, we have also deemed interesting to check whether this mismatch can be translated into a deviation from the Etherington relation. We have applied a calibrator- and model-independent approach previously used by Tonghua et al. (2023) that lets us obtain constraints on the violation of the distance-duality relation. This is the first time this method is applied using BAO data, and also the first time that the robustness of the Etherington relation is studied using angular BAO. Our constraints are quite loose. They allow for violations of $\sim 20\%$ below $z \sim 0.8 - 1$, and even greater at larger redshifts. We do not find any evidence for departures from the standard scenario neither in the anisotropic nor the 2D BAO data sets. The maximum incompatibility with the DDR is found to exist at $\sim 1\sigma$ C.L. in some redshift ranges for the 3D_DESI and 2D_BAO data sets, which is not significant at all. Stronger constraints have been obtained in the literature, but they typically require the use of parametrizations of $\eta(z)$ and, hence, additional assumptions to those considered in this Letter.

In the era of precision cosmology and the existing tensions afflicting the standard Λ CDM model, it is crucial to elucidate what is causing the discrepancies between the various BAO data sets. This is pivotal to find out, for instance, the origin of the Hubble tension (Camarena and Marra, 2020; Gómez-Valent et al., 2024). It will be important to re-assess the level of tension between angular and anisotropic BAO once the new data releases from DESI and future data from Euclid become available. Hopefully, these surveys will provide both 3D and 2D BAO data, extracted by the same collaborations. This would be extremely healthy and useful for the community in order to test

both methods and pinpoint possible sources of biases. In this Letter we have presented a model- and calibrator-independent methodology that can be applied in these future works.

Acknowledgements

AF and MM acknowledge support from the INFN project “InDark”. AGV is funded by “la Caixa” Foundation (ID 100010434) and the European Union’s Horizon 2020 research and innovation programme under the Marie Skłodowska-Curie grant agreement No 847648, with fellowship code LCF/BQ/PI21/11830027. He is grateful to the Institute of Cosmology and Gravitation of the University of Portsmouth for its kind hospitality during the writing of this paper. MM is also supported by the ASI/LiteBIRD grant n. 2020-9-HH.0 and by the Italian Research Center on High Performance Computing Big Data and Quantum Computing (ICSC), project funded by European Union - NextGenerationEU - and National Recovery and Resilience Plan (NRRP) - Mission 4 Component 2 within the activities of Spoke 3 (Astrophysics and Cosmos Observations). AF and AGV acknowledge the participation in the COST Action CA21136 “Addressing observational tensions in cosmology with systematics and fundamental physics” (CosmoVerse).

References

Abbott, T.M.C., et al. (Kilo-Degree Survey, Dark Energy Survey), 2023. DES Y3 + KiDS-1000: Consistent cosmology combining cosmic shear surveys. *Open J. Astrophys.* 6, 2305.17173. doi:10.21105/astro.2305.17173, arXiv:2305.17173.

Abbott, T.M.C., et al. (DES), 2024. Dark Energy Survey: A 2.1% measurement of the angular Baryonic Acoustic Oscillation scale at redshift $z_{\text{eff}}=0.85$ from the final dataset arXiv:2402.10696.

Adame, A.G., et al. (DESI), 2024a. DESI 2024 III: Baryon Acoustic Oscillations from Galaxies and Quasars arXiv:2404.03000.

Adame, A.G., et al. (DESI), 2024b. DESI 2024 IV: Baryon Acoustic Oscillations from the Lyman Alpha Forest arXiv:2404.03001.

Adame, A.G., et al. (DESI), 2024c. DESI 2024 VI: Cosmological Constraints from the Measurements of Baryon Acoustic Oscillations arXiv:2404.03002.

Adil, S.A., Mukhopadhyay, U., Sen, A.A., Vagnozzi, S., 2023. Dark energy in light of the early JWST observations: case for a negative cosmological constant? *JCAP* 10, 072. doi:10.1088/1475-7516/2023/10/072, arXiv:2307.12763.

Aghanim, N., et al. (Planck), 2020. Planck 2018 results. VI. Cosmological parameters. *Astron. Astrophys.* 641, A6. doi:10.1051/0004-6361/201833910, arXiv:1807.06209.

Aiola, S., et al. (ACT), 2020. The Atacama Cosmology Telescope: DR4 Maps and Cosmological Parameters. *JCAP* 12, 047. doi:10.1088/1475-7516/2020/12/047, arXiv:2007.07288.

Akarsu, Ö., Di Valentino, E., Kumar, S., Nunes, R.C., Vazquez, J.A., Yadav, A., 2023. Λ_s CDM model: A promising scenario for alleviation of cosmological tensions arXiv:2307.10899.

Alam, S., et al. (eBOSS), 2021. Completed SDSS-IV extended Baryon Oscillation Spectroscopic Survey: Cosmological implications from two decades of spectroscopic surveys at the Apache Point Observatory. *Phys. Rev. D* 103, 083533. doi:10.1103/PhysRevD.103.083533, arXiv:2007.08991.

Alcaniz, J.S., Carvalho, G.C., Bernui, A., Carvalho, J.C., Benetti, M., 2017. Measuring baryon acoustic oscillations with angular two-point correlation function. *Fundam. Theor. Phys.* 187, 11–19. doi:10.1007/978-3-319-51700-1_2, arXiv:1611.08458.

Aleasant, G., Camarena, D., Di Valentino, E., Kazantzidis, L., Marra, V., Nesseris, S., Perivolaropoulos, L., 2022. Late-transition versus smooth $H(z)$ -deformation models for the resolution of the Hubble crisis. *Phys. Rev. D* 105, 063538. doi:10.1103/PhysRevD.105.063538, arXiv:2110.04336.

Aleasant, G., Kazantzidis, L., Perivolaropoulos, L., 2021. $w - M$ phantom transition at $z_t < 0.1$ as a resolution of the Hubble tension. *Phys. Rev. D* 103, 083517. doi:10.1103/PhysRevD.103.083517, arXiv:2012.13932.

Amendola, L., 1996. Non-gaussian chi-squared method with the multivariate edgeworth expansion. *Astrophys. Lett. Commun.* 33, 63. arXiv:astro-ph/9810198.

Anchordoqui, L.A., Antoniadis, I., Lust, D., Noble, N.T., Soriano, J.F., 2024. From infinite to infinitesimal: Using the Universe as a dataset to probe Casimir corrections to the vacuum energy from fields inhabiting the dark dimension arXiv:2404.17334.

Anselmi, S., Corasaniti, P.S., Sánchez, A.G., Starkman, G.D., Sheth, R.K., Zehavi, I., 2019. Cosmic distance inference from purely geometric BAO methods: Linear Point standard ruler and Correlation Function Model Fitting. *Phys. Rev. D* 99, 123515. doi:10.1103/PhysRevD.99.123515, arXiv:1811.12312.

Avgoustidis, A., Burrage, C., Redondo, J., Verde, L., Jimenez, R., 2010. Constraints on cosmic opacity and beyond the standard model physics from cosmological distance measurements. *JCAP* 10, 024. doi:10.1088/1475-7516/2010/10/024, arXiv:1004.2053.

Benevento, G., Hu, W., Raveri, M., 2020. Can Late Dark Energy Transitions Raise the Hubble constant? *Phys. Rev. D* 101, 103517. doi:10.1103/PhysRevD.101.103517, arXiv:2002.11707.

Bernal, J.L., Smith, T.L., Boddy, K.K., Kamionkowski, M., 2020. Robustness of baryon acoustic oscillation constraints for early-Universe modifications of Λ CDM cosmology. *Phys. Rev. D* 102, 123515. doi:10.1103/PhysRevD.102.123515, arXiv:2004.07263.

Bernal, J.L., Verde, L., Riess, A.G., 2016. The trouble with H_0 . *JCAP* 10, 019. doi:10.1088/1475-7516/2016/10/019, arXiv:1607.05617.

Bernui, A., Di Valentino, E., Giarè, W., Kumar, S., Nunes, R.C., 2023. Exploring the H_0 tension and the evidence for dark sector interactions from 2D BAO measurements. *Phys. Rev. D* 107, 103531. doi:10.1103/PhysRevD.107.103531, arXiv:2301.06097.

du Mas des Bourboux, H., et al., 2020. The Completed SDSS-IV Extended Baryon Oscillation Spectroscopic Survey: Baryon Acoustic Oscillations with $\text{Ly}\alpha$ Forests. *Astrophys. J.* 901, 153. doi:10.3847/1538-4357/abb085, arXiv:2007.08995.

Bousis, D., Perivolaropoulos, L., 2024. Hubble tension tomography: BAO vs SnIa distance tension arXiv:2405.07039.

Brout, D., et al., 2022. The Pantheon+ Analysis: Cosmological Constraints. *Astrophys. J.* 938, 110. doi:10.3847/1538-4357/ac8e04, arXiv:2202.04077.

Camarena, D., Marra, V., 2020. A new method to build the (inverse) distance ladder. *Mon. Not. Roy. Astron. Soc.* 495, 2630–2644. doi:10.1093/mnras/staa770, arXiv:1910.14125.

Camarena, D., Marra, V., 2021. On the use of the local prior on the absolute magnitude of Type Ia supernovae in cosmological inference. *Mon. Not. Roy. Astron. Soc.* 504, 5164–5171. doi:10.1093/mnras/stab1200, arXiv:2101.08641.

Carlioni, Y., Luongo, O., Muccino, M., 2024. Does dark energy really revive using DESI 2024 data? arXiv:2404.12068.

Carosi, G., Friedland, A., Giannotti, M., Pivovarov, M.J., Ruz, J., Vogel, J.K., 2013. Probing the axion-photon coupling: phenomenological and experimental perspectives. A snowmass white paper, in: Snowmass 2013: Snowmass on the Mississippi. arXiv:1309.7035.

Carter, P., Beutler, F., Percival, W.J., DeRose, J., Wechsler, R.H., Zhao, C., 2020. The impact of the fiducial cosmology assumption on BAO distance scale measurements. *Mon. Not. Roy. Astron. Soc.* 494, 2076–2089. doi:10.1093/mnras/staa761, arXiv:1906.03035.

de Carvalho, E., Bernui, A., Avila, F., Novaes, C.P., Nogueira-Cavalcante, J.P., 2021. BAO angular scale at $z_{\text{eff}} = 0.11$ with the SDSS blue galaxies. *Astron. Astrophys.* 649, A20. doi:10.1051/0004-6361/202039936, arXiv:2103.14121.

de Carvalho, E., Bernui, A., Carvalho, G.C., Novaes, C.P., Xavier, H.S., 2018. Angular Baryon Acoustic Oscillation measure at $z = 2.225$ from the SDSS quasar survey. *JCAP* 04, 064. doi:10.1088/1475-7516/2018/04/064, arXiv:1709.00113.

- Carvalho, G.C., Bernui, A., Benetti, M., Carvalho, J.C., Alcaniz, J.S., 2016. Baryon Acoustic Oscillations from the SDSS DR10 galaxies angular correlation function. *Phys. Rev. D* 93, 023530. doi:10.1103/PhysRevD.93.023530, arXiv:1507.08972.
- Carvalho, G.C., Bernui, A., Benetti, M., Carvalho, J.C., de Carvalho, E., Alcaniz, J.S., 2020. The transverse baryonic acoustic scale from the SDSS DR11 galaxies. *Astrophys. J.* 119, 102432. doi:10.1016/j.astropartphys.2020.102432, arXiv:1709.00271.
- Cole, S., et al. (2dFGRS), 2005. The 2dF Galaxy Redshift Survey: Power-spectrum analysis of the final dataset and cosmological implications. *Mon. Not. Roy. Astron. Soc.* 362, 505–534. doi:10.1111/j.1365-2966.2005.09318.x, arXiv:astro-ph/0501174.
- Colgáin, E.O., Dainotti, M.G., Capozziello, S., Pourojaghi, S., Sheikh-Jabbari, M.M., Stojkovic, D., 2024. Does DESI 2024 Confirm Λ CDM? arXiv:2404.08633.
- Efstathiou, G., 2021. To H_0 or not to H_0 ? *Mon. Not. Roy. Astron. Soc.* 505, 3866–3872. doi:10.1093/mnras/stab1588, arXiv:2103.08723.
- Eisenstein, D.J., et al. (SDSS), 2005. Detection of the Baryon Acoustic Peak in the Large-Scale Correlation Function of SDSS Luminous Red Galaxies. *Astrophys. J.* 633, 560–574. doi:10.1086/466512, arXiv:astro-ph/0501171.
- Etherington, I., 1933. On the definition of distance in general relativity. *Philos. Mag.* 15, 761. doi:10.1080/14786443309462220.
- Favale, A., Gómez-Valent, A., Migliaccio, M., 2023. Cosmic chronometers to calibrate the ladders and measure the curvature of the Universe. A model-independent study. *Mon. Not. Roy. Astron. Soc.* 523, 3406–3422. doi:10.1093/mnras/stad1621, arXiv:2301.09591.
- Feeney, S.M., Peiris, H.V., Williamson, A.R., Nissanke, S.M., Mortlock, D.J., Alsing, J., Scolnic, D., 2019. Prospects for resolving the Hubble constant tension with standard sirens. *Phys. Rev. Lett.* 122, 061105. doi:10.1103/PhysRevLett.122.061105, arXiv:1802.03404.
- Gil-Marín, H., Percival, W.J., Verde, L., Brownstein, J.R., Chuang, C.H., Kitchner, F.S., Rodríguez-Torres, S.A., Olmstead, M.D., 2017. The clustering of galaxies in the SDSS-III baryon oscillation spectroscopic survey: RSD measurement from the power spectrum and bispectrum of the DR12 BOSS galaxies. *Mon. Not. Roy. Astron. Soc.* 465, 1757–1788. URL: <https://doi.org/10.1093/mnras/stw2679>, doi:10.1093/mnras/stw2679.
- Gómez-Valent, A., Favale, A., Migliaccio, M., Sen, A.A., 2024. Late-time phenomenology required to solve the H_0 tension in view of the cosmic ladders and the anisotropic and angular BAO datasets. *Phys. Rev. D* 109, 023525. doi:10.1103/PhysRevD.109.023525, arXiv:2309.07795.
- Gómez-Valent, A., Solà Peracaula, J., 2024. Phantom matter: a challenging solution to the cosmological tensions arXiv:2404.18845.
- Gupta, R.P., 2023. JWST early Universe observations and Λ CDM cosmology. *Mon. Not. Roy. Astron. Soc.* 524, 3385–3395. doi:10.1093/mnras/stad2032, arXiv:2309.13100.
- Heisenberg, A., Blake, C., Wiltshire, D.L., 2020. Quantifying the accuracy of the Alcock-Paczynski scaling of baryon acoustic oscillation measurements. *JCAP* 01, 038. doi:10.1088/1475-7516/2020/01/038, arXiv:1908.11508.
- Heisenberg, L., Villarrubia-Rojó, H., Zosso, J., 2022. Can late-time extensions solve the H_0 and σ_8 tensions? *Phys. Rev. D* 106, 043503. doi:10.1103/PhysRevD.106.043503, arXiv:2202.01202.
- Hou, J., et al., 2020. The Completed SDSS-IV extended Baryon Oscillation Spectroscopic Survey: BAO and RSD measurements from anisotropic clustering analysis of the Quasar Sample in configuration space between redshift 0.8 and 2.2. *Mon. Not. Roy. Astron. Soc.* 500, 1201–1221. doi:10.1093/mnras/staa3234, arXiv:2007.08998.
- Huang, L., Wang, S.J., Yu, W.W., 2024. No-go guide for the Hubble tension: late-time or local-scale new physics arXiv:2401.14170.
- Jaeckel, J., Ringwald, A., 2010. The Low-Energy Frontier of Particle Physics. *Ann. Rev. Nucl. Part. Sci.* 60, 405–437. doi:10.1146/annurev.nucl.012809.104433, arXiv:1002.0329.
- Lee, S., 2021. The minimally extended Varying Speed of Light (meVSL). *JCAP* 08, 054. doi:10.1088/1475-7516/2021/08/054, arXiv:2011.09274.
- Lemos, P., Lee, E., Efstathiou, G., Gratton, S., 2019. Model independent $H(z)$ reconstruction using the cosmic inverse distance ladder. *Mon. Not. Roy. Astron. Soc.* 483, 4803–4810. doi:10.1093/mnras/sty3082, arXiv:1806.06781.
- Ma, C., Corasaniti, P.S., 2018. Statistical Test of Distance–Duality Relation with Type Ia Supernovae and Baryon Acoustic Oscillations. *Astrophys. J.* 861, 124. doi:10.3847/1538-4357/aac88f, arXiv:1604.04631.
- Marra, V., Perivolaropoulos, L., 2021. Rapid transition of G_{eff} at $z_t \approx 0.01$ as a possible solution of the Hubble and growth tensions. *Phys. Rev. D* 104, L021303. doi:10.1103/PhysRevD.104.L021303, arXiv:2102.06012.
- Martinelli, M., et al. (EUCLID), 2020. Euclid: Forecast constraints on the cosmic distance duality relation with complementary external probes. *Astron. Astrophys.* 644, A80. doi:10.1051/0004-6361/202039078, arXiv:2007.16153.
- Menci, N., Adil, S.A., Mukhopadhyay, U., Sen, A.A., Vagnozzi, S., 2024. Negative cosmological constant in the dark energy sector: tests from JWST photometric and spectroscopic observations of high-redshift galaxies arXiv:2401.12659.
- More, S., Bovy, J., Hogg, D.W., 2009. Cosmic transparency: A test with the baryon acoustic feature and type Ia supernovae. *Astrophys. J.* 696, 1727–1732. doi:10.1088/0004-637X/696/2/1727, arXiv:0810.5553.
- Moresco, M., et al., 2022. Unveiling the Universe with emerging cosmological probes. *Living Rev. Rel.* 25, 6. doi:10.1007/s41114-022-00040-z, arXiv:2201.07241.
- Nair, R., Jhingan, S., Jain, D., 2012. Cosmic distance duality and cosmic transparency. *JCAP* 12, 028. doi:10.1088/1475-7516/2012/12/028, arXiv:1210.2642.
- Padmanabhan, T., 2003. Cosmological constant: The Weight of the vacuum. *Phys. Rept.* 380, 235–320. doi:10.1016/S0370-1573(03)00120-0, arXiv:hep-th/0212290.
- Pan, J., Huterer, D., Andrade-Oliveira, F., Avestruz, C., 2023. Compressed baryon acoustic oscillation analysis is robust to modified-gravity models arXiv:2312.05177.
- Peebles, P.J.E., Ratra, B., 2003. The Cosmological Constant and Dark Energy. *Rev. Mod. Phys.* 75, 559–606. doi:10.1103/RevModPhys.75.559, arXiv:astro-ph/0207347.
- Perivolaropoulos, L., 2022. Is the Hubble Crisis Connected with the Extinction of Dinosaurs? *Universe* 8, 263. doi:10.3390/universe8050263, arXiv:2201.08997.
- Perivolaropoulos, L., Skara, F., 2022. A Reanalysis of the Latest SH0ES Data for H_0 : Effects of New Degrees of Freedom on the Hubble Tension. *Universe* 8, 502. doi:10.3390/universe8100502, arXiv:2208.11169.
- Perlmutter, S., et al. (Supernova Cosmology Project), 1999. Measurements of Ω and Λ from 42 high redshift supernovae. *Astrophys. J.* 517, 565–586. doi:10.1086/307221, arXiv:astro-ph/9812133.
- Qi, J.Z., Cao, S., Zheng, C., Pan, Y., Li, Z., Li, J., Liu, T., 2019. Testing the Etherington distance duality relation at higher redshifts: Combined radio quasar and gravitational wave data. *Phys. Rev. D* 99, 063507. doi:10.1103/PhysRevD.99.063507, arXiv:1902.01988.
- Qin, J., Melia, F., Zhang, T.J., 2021. Test of the cosmic distance duality relation for arbitrary spatial curvature. *Mon. Not. Roy. Astron. Soc.* 502, 3500–3509. doi:10.1093/mnras/stab124, arXiv:2101.05574.
- Rasmussen, C.E., Williams, C.K.I., 2006. Gaussian Processes for Machine Learning. MIT Press.
- Renzi, F., Hogg, N.B., Giarè, W., 2022. The resilience of the Etherington–Hubble relation. *Mon. Not. Roy. Astron. Soc.* 513, 4004–4014. doi:10.1093/mnras/stac1030, arXiv:2112.05701.
- Riess, A.G., et al. (Supernova Search Team), 1998. Observational evidence from supernovae for an accelerating universe and a cosmological constant. *Astron. J.* 116, 1009–1038. doi:10.1086/300499, arXiv:astro-ph/9805201.
- Riess, A.G., et al., 2022. A Comprehensive Measurement of the Local Value of the Hubble Constant with 1 km/s/Mpc Uncertainty from the Hubble Space Telescope and the SH0ES Team. *Astrophys. J. Lett.* 934, L7. doi:10.3847/2041-8213/ac5c5b, arXiv:2112.04510.
- Rubin, D., et al., 2023. Union Through UNITY: Cosmology with 2,000 SNe Using a Unified Bayesian Framework arXiv:2311.12098.
- Ruchika, Rathore, H., Roy Choudhury, S., Rentala, V., 2023. A gravitational constant transition within cepheids as supernovae calibrators can solve the Hubble tension arXiv:2306.05450.
- Sanz-Wuhl, S., Gil-Marín, H., Cuesta, A.J., Verde, L., 2024. BAO cosmology in non-spatially flat background geometry with application to BOSS and eBOSS arXiv:2402.03427.
- Scolnic, D., et al., 2022. The Pantheon+ Analysis: The Full Data Set and Light-curve Release. *Astrophys. J.* 938, 113. doi:10.3847/1538-4357/ac8b7a, arXiv:2112.03863.
- Seikel, M., Clarkson, C., Smith, M., 2012. Reconstruction of dark energy and

- expansion dynamics using Gaussian processes. *JCAP* 06, 036. doi:10.1088/1475-7516/2012/06/036, [arXiv:1204.2832](#).
- Sánchez, E., Carnero, A., García-Bellido, J., Gaztañaga, E., de Simoni, F., Crocce, M., Cabre, A., Fosalba, P., Alonso, D., 2011. Tracing The Sound Horizon Scale With Photometric Redshift Surveys. *Mon. Not. Roy. Astron. Soc.* 411, 277–288. doi:10.1111/j.1365-2966.2010.17679.x, [arXiv:1006.3226](#).
- Tonghua, L., Shuo, C., Shuai, M., Yuting, L., Chenfa, Z., Jieci, W., 2023. What are recent observations telling us in light of improved tests of distance duality relation? *Phys. Lett. B* 838, 137687. doi:10.1016/j.physletb.2023.137687, [arXiv:2301.02997](#).
- Turner, M.S., 2022. The Road to Precision Cosmology. *Annu. Rev. Nucl. Part. Sci.* 2022 72, 1–35. doi:10.1146/annurev-nucl-111119-041046, [arXiv:2201.04741](#). [arXiv:2201.04741](#).
- Tutusaus, I., Kunz, M., Favre, L., 2023. Solving the Hubble tension at intermediate redshifts with dynamical dark energy [arXiv:2311.16862](#).
- Vincenzi, M., et al. (DES), 2024. The Dark Energy Survey Supernova Program: Cosmological Analysis and Systematic Uncertainties [arXiv:2401.02945](#).
- Wang, D., 2024. The Self-Consistency of DESI Analysis and Comment on "Does DESI 2024 Confirm Λ CDM?" [arXiv:2404.13833](#).
- Wojtak, R., Hjorth, J., 2024. Consistent extinction model for type Ia supernovae in Cepheid-based calibration galaxies and its impact on H_0 [arXiv:2403.10388](#).
- Wojtak, R., Hjorth, J., Hjortlund, J.O., 2023. Two-population Bayesian hierarchical model of Type Ia supernovae. *Mon. Not. Roy. Astron. Soc.* 525, 5187–5203. doi:10.1093/mnras/stad2590, [arXiv:2302.01906](#).